MCL1 is Required for Maintenance of Intestinal Homeostasis and Prevention of Carcinogenesis in Mice

Healy, Marc E ; Boege, Yannick ; Hodder, Michael C ; Böhm, Friederike ; Malehmir, Mohsen ; Scherr, Anna-Lena ; Jetzer, Jasna ; Chan, Lap Kwan ; Parrotta, Rossella ; Jacob, Kurt ; Clerbaux, Laure-Alix ; Kreutzer, Susanne ; Rodewald, Ann-Katrin ; Honcharova-Biletska, Hanna ; Schimmer, Roman ; Büeler, Simone ; Weber, Achim

Abstract: BACKGROUND AIMS Intestinal epithelial homeostasis depends on a tightly regulated balance between intestinal epithelial cell (IEC) death and proliferation. Disruption of factors that promote IEC death result in intestinal inflammation, whereas loss of anti-apoptotic proteins, such as BCL2 or its family member BCL2L1, has no effect on intestinal homeostasis in mice. We investigated the functions of the anti-apoptotic protein MCL1, another member of the BCL2 family, in intestinal homeostasis in mice. METHODS We generated mice with IEC-specific disruption of Mcl1 (Mcl1^{IEC} mice) or tamoxifen-inducible IEC-specific disruption of Mcl1 (i-Mcl1^{IEC} mice); these mice and mice with full-length Mcl1 (controls) were raised under normal or germ-free conditions. Some mice were given antibiotics in their drinking water or the PORCUPINE WNT inhibitor WNT974. Mice were analyzed by endoscopy and for intestinal epithelial barrier permeability. Intestinal tissues were analyzed by histology, in situ hybridization, proliferation assays, and immunoblots. Levels of calprotectin, a marker of intestinal inflammation, were measured in intestinal tissues and feces. RESULTS Mcl1^{IEC} mice spontaneously developed apoptotic enterocolopathy, characterized by increased IEC apoptosis, hyperproliferative crypts, epithelial barrier dysfunction, and chronic inflammation. Loss of MCL1 retained intestinal crypts in a hyperproliferated state and prevented the differentiation of intestinal stem cells. Proliferation of intestinal stem cells in MCL1-deficient mice required WNT signaling and was associated with DNA damage accumulation. By 1 year of age, Mcl1^{IEC} mice developed intestinal tumors with morphologic and genetic features of human adenomas and carcinomas. Germ-free housing of Mcl1^{IEC} mice reduced markers of microbiota-induced intestinal inflammation but not tumor development. CONCLUSION The anti-apoptotic protein MCL1, a member of the BCL2 family, is required for maintenance of intestinal homeostasis and prevention of carcinogenesis in mice. Loss of MCL1 results in development of intestinal carcinomas, even under germ-free conditions, and therefore does not involve microbe-induced chronic inflammation. Mcl1^{IEC} mice might be used to study apoptotic enterocolopathy and inflammatory bowel diseases.

DOI: https://doi.org/10.1053/j.gastro.2020.03.017

Originally published at:
Healy, Marc E; Boege, Yannick; Hodder, Michael C; Böhm, Friederike; Malehmir, Mohsen; Scherr, Anna-Lena; Jetzer, Jasna; Chan, Lap Kwan; Parrotta, Rossella; Jacob, Kurt; Clerbaux, Laure-Alix; Kreutzer, Susanne; Rodewald, Ann-Katrin; Honcharova-Biletska, Hanna; Schimmer, Roman; Büeler, Simone; Weber, Achim (2020). MCL1 is Required for Maintenance of Intestinal Homeostasis and Prevention of Carcinogenesis in Mice. Gastroenterology, 159(1):183-199.
DOI: https://doi.org/10.1053/j.gastro.2020.03.017

Journal Pre-proof

MCL1 is Required for Maintenance of Intestinal Homeostasis and Prevention of Carcinogenesis in Mice

Marc E. Healy, Yannick Boege, Michael C. Hodder, Friederike Böhm, Mohsen Malehmir, Anna-Lena Scherr, Jasna Jetzer, Lap Kwan Chan, Rossella Parrotta, Kurt Jacob, Laure-Alix Clerbaux, Susanne Kreutzer, Andrew Campbell, Ella Gilchrist, Kathryn Gilroy, Ann-Katrin Rodewald, Hanna Honcharova-Biletska, Roman Schimmer, Karelia Vélez, Simone Büeler, Patrizia Cammareri, Gabriela Kalna, Anna S. Wenning, Kathy D. McCoy, Mercedes Gomez de Agüero, Henning Schulze-Bergkamen, Christoph Klose, Kristian Unger, Andrew J. Macpherson, Andreas E. Moor, Bruno Köhler, Owen J. Sansom, Mathias Heikenwalder, Achim Weber

PII: S0016-5085(20)30338-3
DOI: https://doi.org/10.1053/j.gastro.2020.03.017
Reference: YGAST 63275

To appear in: *Gastroenterology*
Accepted Date: 10 March 2020

Please cite this article as: Healy ME, Boege Y, Hodder MC, Böhm F, Malehmir M, Scherr A-L, Jetzer J, Chan LK, Parrotta R, Jacob K, Clerbaux L-A, Kreutzer S, Campbell A, Gilchrist E, Gilroy K, Rodewald A-K, Honcharova-Biletska H, Schimmer R, Vélez K, Büeler S, Cammareri P, Kalna G, Wenning AS, McCoy KD, Gomez de Agüero M, Schulze-Bergkamen H, Klose C, Unger K, Macpherson AJ, Moor AE, Köhler B, Sansom OJ, Heikenwalder M, Weber A, MCL1 is Required for Maintenance of Intestinal Homeostasis and Prevention of Carcinogenesis in Mice, *Gastroenterology* (2020), doi: https://doi.org/10.1053/j.gastro.2020.03.017.

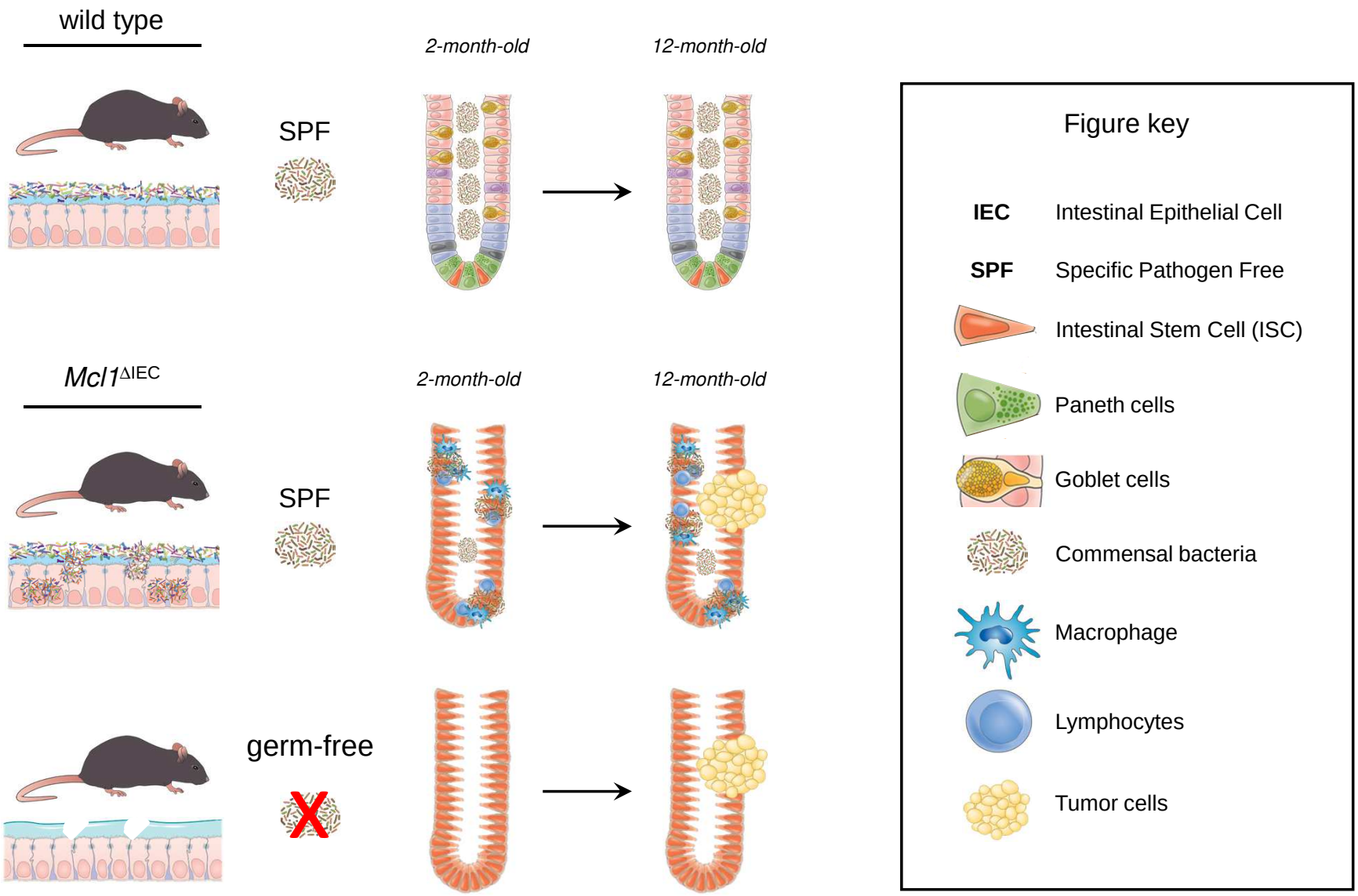
wild type
2-month-old
12-month-old
SPF
Mcl1ΔIEC
2-month-old
12-month-old
SPF
germ-free
X
Figure key
IEC
Intestinal Epithelial Cell
SPF
Specific Pathogen Free
Intestinal Stem Cell (ISC)
Paneth cells
Goblet cells
Commensal bacteria
Macrophage
Lymphocytes
Tumor cells

MCL1 is Required for Maintenance of Intestinal Homeostasis and Prevention of Carcinogenesis in Mice

MCL-1 is indispensable for intestinal homeostasis

Marc E. Healy[1,2,11], Yannick Boege[1,11], Michael C. Hodder[3,9,11], Friederike Böhm[1], Mohsen Malehmir[1], Anna-Lena Scherr[4], Jasna Jetzer[1], Lap Kwan Chan[1], Rossella Parrotta[1], Kurt Jacob[2], Laure-Alix Clerbaux[1,2], Susanne Kreutzer[1], Andrew Campbell[3], Ella Gilchrist[3], Kathryn Gilroy[3], Ann-Katrin Rodewald[1], Hanna Honcharova-Biletska[1], Roman Schimmer[1], Karelia Vélez[2], Simone Büeler[1], Patrizia Cammareri[3], Gabriela Kalna[3], Anna S. Wenning[5], Kathy D. McCoy[5,6], Mercedes Gomez de Agüero[5], Henning Schulze-Bergkamen[4], Christoph Klose[7], Kristian Unger[8], Andrew J. Macpherson[5], Andreas E. Moor[2], Bruno Köhler[4], Owen J. Sansom[3,9,12], Mathias Heikenwalder[10,12], Achim Weber[1,2,12]

Authors' Affiliations

1. Department of Pathology and Molecular Pathology, University Hospital Zurich, 8091 Zurich, Switzerland
2. Institute of Molecular Cancer Research, University of Zurich, 8057 Zurich, Switzerland
3. Cancer Research UK Beatson Institute, Garscube Estate, Bearsden, Glasgow, G61 1BD, UK
4. National Center for Tumor Diseases, Department of Medical Oncology and Heidelberg University Hospital, Internal Medicine VI, Heidelberg, Germany
5. Maurice Müller Laboratories (DKF), Universitätsklinik für Viszerale Chirurgie und Medizin Inselspital, Murtenstrasse 35, University of Bern, Bern, Switzerland
6. Department of Physiology and Pharmacology and Calvin, Phoebe and Joan Snyder Institute for Chronic Diseases, Cumming School of Medicine, University of Calgary, Calgary, Alberta, Canada

7. Department of Medical Microbiology and Hygiene, Institute of Medical Microbiology and Hygiene, University of Freiburg Medical Centre, Freiburg, Germany
8. Research Unit of Radiation Cytogenetics, Helmholtz Zentrum München, Neuherberg Germany
9. Institute of Cancer Sciences, University of Glasgow, Garscube Estate, Glasgow, G61 1QH, UK
10. Division of Chronic Inflammation and Cancer, Deutsches Krebs-Forschungszentrum (DKFZ), 69120 Heidelberg, Germany
11. contributed equally and shared first authors
12. shared last and corresponding authors

Grant support

A.W. was supported by grants from the Swiss National Science Foundation (SNF 310030_146940), from the Krebsliga Zurich, and the Vontobel Stiftung Zurich, Switzerland. H.S.B. was supported by a grant from the Deutsche Forschungsgemeinschaft (DFG, SCHU 1443 4-1). H.M. was supported by an ERC consolidator grant (Hepatometabopath), an ERC Horizon 2020 (HEP-CAR) grant, the SFBTR 179, 209, 1335 and a grant by the Wilhelm-Sander Stiftung. O.J.S. was supported by an ERC starting grant (311301-ColonCan). O.J.S. and P.C. were supported by a Cancer Research UK core grant (A21139 and A17196). M.C.H. was supported by an MRC doctoral training grant (MR/J50032x/1). B.K. was supported by grants DKH70113426, DFG KO 5205/1-1 and a Brigitte und Dr. Konstanze Wegener-Stiftung.

Corresponding authors

Achim Weber, Department of Pathology and Molecular Pathology, University Hospital Zurich, 8091 Zurich, Switzerland; phone: +41-44-2552781; achim.weber@usz.ch

Mathias Heikenwälder, Division of Chronic Inflammation and Cancer, German Cancer Research Center (DKFZ), 69120 Heidelberg, Germany, phone: +49-6221-423891; m.heikenwaelder@dkfz.de

Owen J. Sansom, Cancer Research UK Beatson Institute, Garscube Estate, Bearsden, and Institute of Cancer Sciences, University of Glasgow, Garscube Estate, Glasgow, UK; o.sansom@beatson.gla.ac.uk

Disclosures

The authors listed above confirm that they have no conflicts of interest to declare.

Transcript Profiling

Sequencing data have been deposited at the European Nucleotide Archive under the accession number PRJEB20295 and PRJEB20400.

Author Contribution

M.E.H., Y.B., M.C.H., O.J.S., M.H., and A.W. conceived and designed the project. M.E.H., Y.B., M.C.H., F.B., M.M., A.L.S., J.J., L.K.C, R.P., K.J., L.A.C., S.K., A.C., E.G., K.G., A.R., H.H., R.S., K.V., S.B., P.C., G.K., A.S.W., A.E.M. performed experiments. All authors analyzed data. M.E.H., Y.B., M.C.H., F.B., M.M. and A.L.S. performed breeding and S.P.F. housing of mice. K.M.C., M.G.A., and A.M. performed germ-free housing of mice. M.E.H., M.H., and A.W. wrote the manuscript, and all authors contributed to writing and provided feedback.

Abstract

Background & Aims

Intestinal epithelial homeostasis depends on a tightly regulated balance between intestinal epithelial cell (IEC) death and proliferation. Disruption of factors that promote IEC death result in intestinal inflammation, whereas loss of anti-apoptotic proteins, such as BCL2 or its family member BCL2L1, has no effect on intestinal homeostasis in mice. We investigated the functions of the anti-apoptotic protein MCL1, another member of the BCL2 family, in intestinal homeostasis in mice.

Methods

We generated mice with IEC-specific disruption of *Mcl1* (*Mcl1*$^{\Delta IEC}$ mice) or tamoxifen-inducible IEC-specific disruption of *Mcl1* (i-*Mcl1*$^{\Delta IEC}$ mice); these mice and mice with full-length *Mcl1* (controls) were raised under normal or germ-free conditions. Some mice were given antibiotics in their drinking water or the PORCUPINE WNT inhibitor WNT974. Mice were analyzed by endoscopy and for intestinal epithelial barrier permeability. Intestinal tissues were analyzed by histology, in situ hybridization, proliferation assays, and immunoblots. Levels of calprotectin, a marker of intestinal inflammation, were measured in intestinal tissues and feces.

Results

Mcl1$^{\Delta IEC}$ mice spontaneously developed apoptotic enterocolopathy, characterized by increased IEC apoptosis, hyperproliferative crypts, epithelial barrier dysfunction, and chronic inflammation. Loss of MCL1 retained intestinal crypts in a hyperproliferated state and prevented the differentiation of intestinal stem cells. Proliferation of intestinal stem cells in MCL1-deficient mice required WNT signaling and was associated with DNA damage accumulation. By 1 year of age, *Mcl1*$^{\Delta IEC}$ mice developed intestinal tumors with morphologic and genetic features of human adenomas and carcinomas. Germ-free housing of *Mcl1*$^{\Delta IEC}$

mice reduced markers of microbiota-induced intestinal inflammation but not tumor development.

Conclusion

The anti-apoptotic protein MCL1, a member of the BCL2 family, is required for maintenance of intestinal homeostasis and prevention of carcinogenesis in mice. Loss of MCL1 results in development of intestinal carcinomas, even under germ-free conditions, and therefore does not involve microbe-induced chronic inflammation. *Mcl1*$^{\Delta IEC}$ mice might be used to study apoptotic enterocolopathy and inflammatory bowel diseases.

KEY WORDS

colorectal carcinoma, CRC, cell death, tumorigenesis

Introduction

Intestinal homeostasis is dependent on a tightly regulated interaction between the epithelium, the immune system and luminal commensal bacteria. The intestinal epithelium compartment is comprised of different cell types including proliferative stem cells as well as highly specialized absorptive (enterocytes) and secretory cells (goblet, Paneth and neuroendocrine cells)[1, 2]. These intestinal epithelial cells (IEC) provide a physical barrier between the intestinal mucosa and potentially pathogenic microorganisms. IEC display a high cell turnover, necessitating a strictly regulated balance of proliferation and cell death to guarantee intestinal epithelial homeostasis[3]. However, excessive IEC death is a well-known clinical hallmark of apoptotic enterocolopathy and inflammatory bowel disease (IBD)[3-5].

In recent years, there has been a great scientific interest in determining the roles played by cell death regulating molecules in maintaining tissue homeostasis and preventing tumorigenesis. Transgenic mice, generated with intestinal specific knockouts of particular IEC circuits of regulated cell death (RCD), FADD, Caspase 8 or RIPK1, display excessive IEC turnover, epithelial defects and IBD-like inflammation[6-11]. In contrast, mice harboring intestinal specific deletions of other RCD-molecules, BCL2 or BCL2L1, display surprisingly little pathology under steady state conditions. Although capable of modulating intestinal carcinogenesis in tumor models, both are dispensable for maintaining intestinal homeostasis[12, 13]. Interestingly, another pro-survival BCL2 family member, MCL1, is essential for maintaining homeostasis in several tissues with regenerative capacity[14-16]. The indispensable role for MCL1 in maintaining liver homeostasis[15, 16] prompted us to study its function in the intestinal tract.

Materials and Methods

Mice: Housing and experimental procedures of all animals were performed in accordance with the Cantonal Veterinary Office (Zurich, Switzerland) under the license numbers ZH217/12 and ZH166/15 or the UK Home Office regulations (licence 70/8646) according to ARRIVE guidelines. Animals were maintained under SPF conditions at the University of Zurich or at the CRUK Beatson Institute, Glasgow. Germ-free housing of mice was performed within the Clean Mouse Facility of the University of Bern[17]. A detailed description of the generation of each mouse line is provided in the Supplemental material.

Antibiotic (ABX) treatment: Ciprofloxacin (200mg/L) (Fluka), Ampicillin Sodium (1g/L) (Sigma), Metronidazole (1g/L) (Fluka) and Vancomycin HCl (500mg/L) (Fluka) were added to the drinking water of co-housed, 1-month-old wild type control and *Mcl1*$^{\Delta IEC}$ mice for 4 weeks[18].

ILC depletion: 2-month-old *Mcl1*$^{\Delta IEC}$*Rag1*$^{-/-}$ mice were treated with α-Thy1.2 depleting antibody (200µg) (BioxCell – clone:30H12) or appropriate isotype control via IP injection, 3 times per week for 4 weeks.

WNT signalling inhibition: i-*Mcl1*$^{\Delta IEC}$ mice or wild type controls received 5mg/kg of WNT974 (provided via an MTA with Novartis) orally, twice per day, in a 0.5% methylcellulose, 0.5% tween 80 vehicle.

BrdU proliferation analysis: BrdU (Amersham Biosciences) was administered via IP injection 2 hours before sacrificing. The number of BrdU positive crypts was determined by

calculating the average number of BrdU positive crypt cells per half crypt from 50 individual crypts.

Intestinal epithelial barrier permeability: Intestinal epithelial barrier permeability was measured using FITC-labelled dextran (FD-4) as previously described[19]. Serum expression of FD-4 was determined using a BioTek Microplate Reader (BioTek).

Endoscopy: Direct visualization of colonic mucosal damage of WT and *Mcl1*$^{\Delta IEC}$ mice was performed via high-resolution endoscopy using a "Coloview system" (Karl Storz, Tuttlingen, Germany). Mice were provided with food and water as normal until the endoscopy was performed. Isoflurane inhalation (2-2.5%) in oxygen was used to anaesthetize the mice for the duration of the procedure.

Calprotectin analysis: Calprotectin (S100A8 and S100A9) levels were determined from homogenates of colon tissue (Real Time PCR) or feces (ELISA). Calprotectin primer sequences: *S100A8* - For AAATCACCATGCCCTCTACAAG and Rev CCCACTTTTATCACCATCGCAA, *S100A9* – For ATACTCTAGGAAGGAAGGACACC and Rev TCCATGATGTCATTTATGAGGGC. Reference gene (*Gapdh)* - For CCACCCCAGCAAGGAGACT and Rev GAAATTGTGAGGGAGATGCT. Protein levels of Calprotectin (S100A8 and S100A9) were determined by ELISA (Immune Diagnostik, #K6936).

Histology: Formalin fixed tissue was embedded in paraffin. Paraffin sections were re-hydrated and heat-induced antigen retrieval was performed in either Tris/EDTA/BORAT or citrate buffer. Incubation in Ventana buffer and staining was performed on a BenchmarkUltra immunohistochemistry robot (Ventana Instruments) using Chromo Map or Optiview Dab

Detection Kits (Ventana) or on a Bond MAX (Leica). All primary antibodies used for immunohistochemistry are listed in Table S2. A detailed description of the criteria used for the histological scoring is available in the Supplemental material (Table S5).

Tumor classification: H&E stained slides of intestinal lesions, blinded for genotype and housing conditions, were independently evaluated by two pathologists. Tumor classification was based on established nomenclature and criteria for the histologic assessment of intestinal tumors in mice[20]. According to the criteria for the classification of human intestinal tumors, a small bowel neoplasm with infiltrative growth in the mucosa was classified as a carcinoma[21]. In cases where mice developed multiple tumors, classification was performed according to the highest lesion.

In situ hybridization: ISH was performed on FFPE tissues according to the manufacturer`s protocol using four commercially available probes. A detailed description of all probes used in this study can be found in the Supplemental material.

Ex vivo cytokine expression analysis: Ex vivo cytokine analysis was performed using supernatant recovered from colon cultures as previously described[22]. Supernatant was collected after 48 hours and cytokine expression was determined using Multiplex analysis kits (Bio-Rad Laboratories) and read using Bio-Plex® MAGPIX™ Multiplex Reader powered by Luminex XMAP Technology (Bio-Rad Laboratories).

Sequencing: Genomic DNA was isolated from FFPE tissue blocks using Macherey & Nagel's NucleoSpin FFPE Kit and analysed by Sanger Sequencing or Whole Exome Sequencing. A detailed description of the sequencing protocols used for are available in the Supplemental material.

RNASeq analysis was performed on RNA extracted from whole small intestine tissue of i-*Mcl1*$^{\Delta IEC}$ mice (4 days post deletion) or i-*Apc*$^{\Delta IEC}$ and i-*Apc*$^{\Delta IEC}$ *Mcl1*$^{\Delta IEC}$ mice (3 days post deletion). A detailed description of the RNASeq protocol is provided in the Supplemental material. GSEA analysis was performed using the GSEA v2.0 software (Broad Institute). The comparison gene sets were obtained from published sources; genes upregulated following APC loss[23] & WNT target genes commonly upregulated in human colorectal cancer[24].

Single molecule FISH (smFISH): smFISH was performed as previously described[25]. A comprehensive description of the protocol, including quantification and probes used (Tables S3-S5), is provided in the Supplemental material.

Statistical analysis: Statistical analyses were conducted as indicated within each figure legend. For all analysis, *$p \leq 0.05$, **$p \leq 0.01$, ***$p \leq 0.001$. Statistical analyses were conducted using GraphPad Prism 5/7 software.

Results

MCL1 is a key regulator of intestinal homeostasis

To unravel the physiological role of MCL1 within the intestinal tract, we generated mice with an IEC-specific deletion of *Mcl1* (*Mcl1*$^{\Delta IEC}$ mice) (Figure S1*A*). Compared with littermate controls, *Mcl1*$^{\Delta IEC}$ mice developed extensive diarrhea, reduced weight gain and significantly increased mortality (Figure 1*A*). Colonoscopies performed on 4-month-old *Mcl1*$^{\Delta IEC}$ mice revealed extensive thickening and whitening of the colonic wall and distinct polyp formation (Figure 1*A*). Furthermore, 2-month-old *Mcl1*$^{\Delta IEC}$ mice displayed an impaired epithelial barrier function, as demonstrated by increased permeability of orally administered FITC-labeled dextran (Figure 1*B*). Elevated levels of S1008/S1009 (calprotectin), a biomarker of intestinal inflammation, were also detected in stool samples and tissue homogenates from *Mcl1*$^{\Delta IEC}$ mice (Figure 1*C*).

Interestingly, not all IEC within *Mcl1*$^{\Delta IEC}$ mice underwent *Mcl1* recombination and subsequently *Mcl1*$^{\Delta IEC}$ mice displayed areas that retained *Mcl1* expression alongside areas of *Mcl1* deficiency. Consequently, areas of severe mucosal damage appeared alongside histologically normal regions of both the small intestine and colon. Interestingly, IEC in histologically normal mucosal regions retained *Mcl1* mRNA expression while IEC from damaged mucosal regions lacked *Mcl1* (Figure 1*D*). Furthermore, S1008/S1009 levels were inversely correlated with *Mcl1* expression, indicating the severity of intestinal damage was closely correlated with *Mcl1* deficiency (Figure S1*B*). Histopathological analysis of 2-month-old *Mcl1*$^{\Delta IEC}$ mice showed architectural disarray with crypt hyperplasia, villous atrophy (small intestine), increased IEC apoptosis (rather than necroptosis) (cleaved caspase 3) and hyperproliferative crypts (Ki-67) throughout both the colon and small intestine (Figures 1*E-F*, S1*C-F*). Notably, deleting a single copy of the *Mcl1* gene was not sufficient to induce the histopathological damage observed in *Mcl1*$^{\Delta IEC}$ mice (Figure S2*A*).

MCL1 deficiency results in microbiota-induced chronic inflammation

In addition to the impaired epithelial barrier function described above, we also observed a marked decrease in the protective mucus layer at the intestinal mucosal barrier as well as extensive bacterial translocation from the lumen into the mucosa in *Mcl1*$^{\Delta IEC}$ mice (Figure S3*A*). Taken together, we concluded that MCL1 deficiency resulted in major epithelial cell dysfunction and chronic intestinal inflammation. Indeed, large lymphoid follicles, comprising mainly B and T cells, as well as an increased number of infiltrating immune cells were detected within the mucosa of *Mcl1*$^{\Delta IEC}$ mice (Figure S4*A*). In addition, pro-inflammatory cytokines TNF-α, IL-22, IL-23A, IL-17A, IL-17F and IL-1β were significantly in *Mcl1*$^{\Delta IEC}$ mice (Figure 1*G* and S4*B*). To determine the contribution of adaptive immune cells to mucosal inflammation and subsequent pathology following *Mcl1* deletion, *Mcl1*$^{\Delta IEC}$ mice were inter-crossed with *Rag1*$^{-/-}$ mice (*Mcl1*$^{\Delta IEC}$*Rag1*$^{-/-}$ mice). Unexpectedly, *Mcl1*$^{\Delta IEC}$*Rag1*$^{-/-}$ mice exhibited significantly reduced weight gain and shorter survival compared to both wild type and *Mcl1*$^{\Delta IEC}$ mice (Figure 2*A*). In addition, *Mcl1*$^{\Delta IEC}$*Rag1*$^{-/-}$ mice also retained increased IEC apoptosis, hyperproliferative crypts, extensive mucosal damage (Figures 2*B-C*, S5*A-B*) and elevated levels of pro-inflammatory cytokines despite lacking conventional T cells (Figures 2*D*, S5*C-D*). Given the observed cytokine profile, we postulated that innate lymphoid cells (ILC)[26] were driving chronic intestinal inflammation, at least in the absence of conventional T cells. To test this hypothesis, ILC were depleted in 2-month-old *Mcl1*$^{\Delta IEC}$*Rag1*$^{-/-}$ mice following a 4-week treatment with α-Thy1.2 antibody. Thy1 (CD90) positive cell depletion (Figure S6*A*) improved MCL1 deficiency-associated damage and resulted in the significant reduction of pro-inflammatory cytokines IL-22 and IL-17F (Figure 2*E-F*, S6*B*). However, increased IEC apoptosis and hyperproliferation persisted after ILC depletion (Figure 2*E*). Thus, by showing that MCL1 is indispensable for intestinal homeostasis, we identified a novel function for MCL1, not observed for family members BCL2 and BCL2L1[12, 13].

Increased IEC apoptosis and hyperproliferation are a direct consequence of *Mcl1* deletion

In order to delineate whether the increased IEC apoptosis and hyperproliferation observed in *Mcl1*$^{\Delta IEC}$ mice were caused by the aforementioned chronic inflammation, or a direct result of MCL1 deficiency, *Mcl1*$^{\Delta IEC}$ mice were either placed under antibiotic treatment (ABX)[18], or re-derived under germ-free conditions[17] (Figure S7*A*-*B*). Following 4 weeks of ABX treatment, 2-month-old *Mcl1*$^{\Delta IEC}$ mice showed attenuated damage and significantly reduced intestinal inflammation compared to untreated *Mcl1*$^{\Delta IEC}$ mice (Figures S8*A*). However, ABX-treated *Mcl1*$^{\Delta IEC}$ mice retained increased IEC apoptosis and hyperproliferative crypts (Figure S8*A*). Similarly, germ-free *Mcl1*$^{\Delta IEC}$ mice displayed increased mucosal healing and a distinct lack of the immune cell infiltration observed in SPF *Mcl1*$^{\Delta IEC}$ mice (Figures 3*A*-*B*, S8*B*-*C* and S9*A*-*B*). *Mcl1* deletion under germ-free conditions did not result in increased pro-inflammatory cytokine production when compared with littermate controls despite evidence suggesting an impaired intestinal epithelial barrier (Figure 3*C*, S8*D*, S10*A*). However, ameliorating chronic intestinal inflammation did not prevent the increased IEC apoptosis or hyperproliferation associated with *Mcl1* deletion (Figures 3*A*, S8*B*). Collectively these data show that whereas MCL1 deficiency related chronic inflammation was due to an uncontrolled immune response against disseminating microbiota, increased IEC apoptosis and hyperproliferation directly result from MCL1 deficiency.

MCL1 is essential for intestinal stem cell homeostasis and differentiation

Morphological analysis of the crypt compartments (Figure 1*E*) suggested that cellular compartmentalization was significantly dysregulated throughout the small intestine and colon of *Mcl1*$^{\Delta IEC}$ mice. Indeed, immunohistochemical analysis revealed that, following *Mcl1* deletion, intestinal stem cells (ISC) were not capable of differentiating towards secretory lineages. *Mcl1*$^{\Delta IEC}$ mice showed a complete loss of both goblet (AB/PAS positive) and Paneth cells (Lysozyme positive) in damaged (MCL1 deficient) areas (Figure 4*A*-*C* and S11*A*). Of

note, in unaffected areas (MCL1 positive), ISC retained their differentiation capabilities, and produced both goblet and Paneth cells at a comparable rate to control mice (Figures 4*B-C*). Impaired ISC differentiation was also observed in affected compartments of germ-free *Mcl1*$^{\Delta IEC}$ mice, delineating the necessity for MCL1 in retaining intestinal homeostasis and ISC differentiation from chronic inflammation.

Interestingly, MCL1 deficient undifferentiated and hyperproliferative cells also retained the ISC markers OLFM4, SOX9 and *Lgr5* (restricted to the base of the crypts under steady state conditions) throughout mid to apical parts of crypts (Figure 4*A* and S11*B*). To elucidate the molecular basis of this impaired ISC differentiation, we focused on the expression of *Atoh1, an* essential transcription factor for the differentiation of ISC towards the secretory cell lineages[27]. Interestingly, we observed a significant reduction in *Atoh1* expression in *Mcl1*-deficient ISC compared to *Mcl1*-positive ISC within the same mouse using single molecule fluorescent in situ hybridization (smFISH) (Figure 4*D-E* and *S12A-B*). These results suggest that, in the absence of MCL1, the axis of ISC proliferation and differentiation is constrained and polarized towards a highly proliferative ISC dominant environment.

Given the well-established connection between hyperproliferation, replicative stress and DNA damage[16, 28], we next sought to look for evidence of DNA damage accumulation. Immunohistochemical staining for the DNA damage response marker γH2AX, revealed strong positivity within the crypts of *Mcl1*$^{\Delta IEC}$ mice. γH2AX positivity was consistently found in *Mcl1*-deficient IEC but not in *Mcl1*-expressing IEC or IEC of littermate controls (Figure S13*A-B*). Furthermore, γH2AX positivity was also observed under germ-free conditions, independent of chronic inflammation. Altogether, MCL1 deficiency restricts ISC to an undifferentiated and hyperproliferative state that makes the ISC susceptible to the accumulation of DNA damage.

MCL1-deficiency associated ISC hyperproliferation is dependent on WNT signaling

To further investigate the direct consequences of *Mcl1* deletion and how it translates to IEC hyperproliferation and loss of differentiation, we generated a tamoxifen-inducible IEC-specific *Mcl1* knockout mouse (i-*Mcl1*$^{\Delta IEC}$ mice). Importantly the phenotype of i-*Mcl1*$^{\Delta IEC}$ mice closely recapitulated the phenotype of *Mcl1*$^{\Delta IEC}$ mice. The epithelium of i-*Mcl1*$^{\Delta IEC}$ mice displayed architectural disarray with crypt hyperplasia, villous atrophy (small intestine), increased IEC apoptosis and IEC hyperproliferation throughout the small intestine and the colon (Figure 5*A*, S14*A*). i-*Mcl1*$^{\Delta IEC}$ mice also displayed impaired epithelial barrier function and a markedly increased immune infiltration (3-4 days post induction) (Figures S14*A*-*C*). ISC differentiation to secretory lineages was also significantly reduced in i-*Mcl1*$^{\Delta IEC}$ mice illustrated by a marked reduction in both goblet and Paneth cells following *Mcl1* deletion (Figure 5*B*). In addition, i-*Mcl1*$^{\Delta IEC}$ mice also displayed strong γH2AX positivity, detectable throughout the small intestine and colon following *Mcl1* deletion (Figure 5*B*). In addition, gene set enrichment analysis (GSEA from RNAseq data), indicated a strong enrichment for genes commonly up-regulated in response to the detection of DNA damage and post-replication DNA repair in i-*Mcl1*$^{\Delta IEC}$ mice compared to littermate controls (Figures 5*C* and S15*A*). These data further corroborated that the γH2AX positivity associated with *Mcl1* deletion was indeed indicative of DNA damage.

i-*Mcl1*$^{\Delta IEC}$ mice displayed complete *Mcl1* recombination throughout the entire intestine (compared to the “patchy” recombination described in *Mcl1*$^{\Delta IEC}$ mice) and so represented a valuable tool by which to more accurately investigate the molecular consequences to *Mcl1* deletion (Figure S16A). Interestingly, i-*Mcl1*$^{\Delta IEC}$ mice displayed a strong activation of wound healing programs and increased expression of WNT target genes as determined by RNASeq analysis (Tables S13 and S14). Moreover, following *Mcl1* deletion, GSEA also indicated an enrichment for genes commonly up-regulated in human colorectal cancer (CRC) as well as mice with an IEC-specific deletion of adenomatous polyposis coli (*Apc*), a prototypical model

for intestinal tumorigenesis[29] (Figures 5*D* and S14*D*). To test whether MCL1 deficiency-associated hyperproliferation observed within the ISC compartment was dependent on WNT signaling, we co-deleted a single copy of the canonical WNT pathway mediator *Ctnnb1* (β-catenin) in conjunction with *Mcl1* (i-*Ctnnb1*$^{\Delta IEC/wt}$*Mcl1*$^{\Delta IEC}$ mice). Deleting a single copy of *Ctnnb1* was sufficient to partially rescue the hyperproliferative phenotype associated with *Mcl1* deletion (Figures 5*E* and S17*A*). Subsequently, i-*Mcl1*$^{\Delta IEC}$ mice were treated with the WNT signaling/porcupine inhibitor WNT974. Strikingly, WNT974 treatment completely ameliorated hyperproliferation within the crypts of both the small intestine and colon of i-*Mcl*1$^{\Delta IEC}$ mice (Figures 5*F*, S17*B* and S18*A*-*B*). Collectively, these data suggest that the impaired intestinal homeostasis following *Mcl1* deletion inflicts a WNT-induced hyperproliferative state on undifferentiated IEC.

To determine whether increased WNT signaling observed following *Mcl1* deletion was a direct or indirect consequence of *Mcl1* deletion, we next used smFISH to visualize *Wnt2b* molecules within the stroma of *Mcl1*$^{\Delta IEC}$ mice. Firstly, *Wnt2b* expression levels were markedly increased within the stroma of damaged areas (*Mcl1*-deficient) compared to unaffected areas (*Mcl1*-expressing) (Figure 5*G* and S19*A*-*B*). Secondly, IEC did not express *Wnt2b* irrespective of *Mcl1* expression. *Wnt2b* expression was completely restricted to the pool of *Mcl1*-positive cells within the stroma surrounding the intestinal crypts (Figure 5*G* and S19*A*-*B*).

In order to delineate a potential effect of MCL1 deficiency in driving IEC proliferation from the effect of increased WNT signaling, we next generated a tamoxifen-inducible knockout mouse which facilitated the simultaneously delete both *Mcl1* and the essential negative regulator of WNT signaling *Apc* (i-*Apc*$^{\Delta IEC}$*Mcl1*$^{\Delta IEC}$ mice). As previously described, *Apc* deletion (i-Apc$^{\Delta IEC}$ mice) resulted in increased crypt proliferation and subsequent hyperplasia as a result of constitutive WNT signaling (Figure 6*A*). Remarkably, co-deletion of *Apc* and *Mcl1* resulted in a further significant increase in crypt proliferation throughout the small intestine and colon (Figure 6*A*). RNAseq analysis from these mice also showed significantly higher expression of

essential proliferation associated genes *Pcna*, *Cdk1*, *Cdk4* and *E2f1*, as well as marked increases in *Ccnd1* and *cMyc*, which was not attributable to activated WNT signaling (Figure 6*B-D* and S20*A-C*). Similar to Mcl1$^{\Delta IEC}$ mice, IEC proliferation was intrinsically linked to increased apoptosis irrespective of the increased WNT signaling (Figure S20*D*). These results demonstrate that even in the presence of constitutive WNT signaling, the loss of *Mcl1* directly increases IEC proliferation beyond the levels obtained by WNT signaling alone.

Despite the clear growth advantage observed in MCL1 deficient ISC in vivo, it was surprisingly not possible to establish a viable line of *Mcl1* deficient organoids from *Mcl1*$^{\Delta IEC}$ mice. Interestingly, while it was possible to establish a low yield of organoids from the small intestine of i-*Mcl1*$^{\Delta IEC}$ mice, the organoids which formed had escaped recombination and retained *Mcl1* expression (Figure 6*E*). Remarkably, organoids derived from the small intestine of i-*Apc*$^{\Delta IEC}$*Mcl1*$^{\Delta IEC}$ mice were viable and retained *Mcl1* deficiency through at least 5 passages (Figure 6*F-G* and S21*A*). These observations suggest that the activation of WNT signaling and subsequent WNT saturated environment is essential for the survival of MCL1 deficient ISC. Collectively, these results not only demonstrate that MCL1 deficiency is intricately linked to an activated WNT signaling pathway, but that a clear proliferation-enhancing effect exists that is directly attributable to MCL1 deficiency.

Mcl1 deficiency results in carcinoma development

Given the increased proliferation and undifferentiated state of MCL1 deficient ISC, together with the intestinal polyps observed in 4-month-old *Mcl1*$^{\Delta IEC}$ mice (Figure 1*A*), we next aimed to monitor the long-term sequelae of MCL1 deficiency. Strikingly, we found that life-long MCL1 deficiency resulted in intestinal tumorigenesis (Figure 7*A*). By one year, >80% of *Mcl1*$^{\Delta IEC}$ mice displayed intestinal neoplasms within the small intestine and/or colon. Remarkably, intestinal tumors developed with similar incidence under both SPF and germ-free conditions, therefore independently of microbe-induced intestinal inflammation (Figure 7*B*). Lesions comprised a spectrum ranging from hyperplastic changes over low and high

grade adenomas to invasive carcinomas[20], thus mirroring Vogelstein`s adenoma-carcinoma-sequence of human intestinal carcinogenesis[30] (Figure 7*C*, S22*A*). Carcinoma found in *Mcl1*$^{\Delta IEC}$ mice extended deep into the *muscularis propria* (black box) and infiltrated intestinal vasculature (black circle) (Figure 7*C*). Of note, tumors were consistently MCL1 deficient and multiclonal in origin as shown by lineage tracing with the multicolor Cre-reporter R26R-Confetti[31] (Figures 7*D* and S22*B*). MCL1 deficient tumors also displayed inter- and intratumoral heterogeneity with respect to differentiation markers such as CD44, CDX2 and synaptophysin (Figure S22*C*). Furthermore, tumors displayed regional *Axin2* positivity and β-catenin nuclear localization indicating responsiveness to active WNT signaling and/or *Ctnnb1* mutations (Figures 7*E-F* and S22*D*).

While progressing through the adenoma-carcinoma-sequence, tumors increasingly displayed genomic alterations in terms of non-recurrent chromosomal aberrations as determined by array comparative genomic hybridization (aCGH), as well as single nucleotide variants (SNV) as determined by whole exome and Sanger sequencing (Figure 7*G*). Remarkably, Synteny analysis revealed a statistically significant overlap of chromosomal gains and losses with those found in human colorectal carcinomas (CRC) (78.3% of gains and 69.8% of losses; Figure 7*H*)[32]. Strikingly, SNV comprised functionally relevant mutations in genes of the WNT pathway frequently also mutated in human CRC such as *CTNNB1, APC, FBXW7 and ARID1*[30, 32, 33] (Figure S23A).

Collectively, these findings demonstrate that carcinogenesis in *Mcl1*$^{\Delta IEC}$ mice morphologically and genetically closely recapitulates human intestinal carcinogenesis[30, 33]. Furthermore, since tumors develop under germ-free conditions, MCL1 deficiency-related tumorigenesis is uncoupled from microbiota-induced chronic inflammation, a well-established promoter of intestinal carcinogenesis[34].

Discussion

In this study, we have identified an essential role for MCL1 in preserving intestinal homeostasis and preventing carcinoma formation, previously undescribed among BCL2 anti-apoptotic family members. These findings, in particular the microbiota-independency of MCL1 deficiency-associated tumorigenesis, clearly demonstrate an essential role for MCL1 in preserving intestinal homeostasis. These results may have important implications for understanding the pathogenesis of apoptotic enterocolopathy, IBD and CRC development.

Disturbances in epithelial barrier integrity with dysfunctional IEC–intrinsic molecular circuits that control tissue homeostasis, renewal, and the repair of IEC are cardinal features of both apoptotic enterocolopathy and IBD. Remarkably, intestinal pathology due to IEC-specific MCL1 deficiency shared hallmark features with IBD, including barrier dysfunction, chronic inflammation, increased IEC apoptosis, hyperproliferation and impaired ISC differentiation[1, 3, 5]. Thus, *Mcl1*$^{\Delta IEC}$ mice may represent a pertinent preclinical model of both apoptotic enterocolopathy and IBD, while also opening up the possibility that (even a temporally restricted) dysregulation of MCL1 may contribute to the development of these, and similar, conditions.

Given the well-established increased risk for IBD patients to develop intestinal carcinomas, which increases parallel to the duration and severity of their disease[35], it was interesting to discover that *Mcl1*$^{\Delta IEC}$ mice also spontaneously developed intestinal carcinomas. Remarkably however, while chronic inflammation has been established as a major driver of intestinal carcinoma[35], MCL1 deficiency-related carcinoma formation was independent of microbe-induced chronic inflammation.

Given the multifaceted and crucial roles of MCL1[36], various mechanisms are conceivable to explain MCL1 deficiency-related tumorigenesis. Of note, tumor lesions observed in *Mcl1*$^{\Delta IEC}$ mice exhibited the full spectrum of human CRC development described by Vogelstein *et al.*[30], ranging from dysplastic crypts and low grade adenoma to high grade adenoma and carcinoma. Interestingly, tumors that developed as a result of MCL1 deficiency not only bear a striking similarity to human CRC, but revealed significant correlations with the subgroup of

CRC characterized by active WNT signaling. These results indicate a potentially direct and immediate function for MCL1 in regulating IEC proliferation and suppressing tumor formation, the functional consequence of which becomes obvious in the presence of constitutive WNT signaling. This scenario not only explains the mutational spectrum observed in MCL1 deficient tumors, with clear enrichment of genes associated with WNT signaling[32], but also explains the differential viability observed in ex vivo organoid cultures derived from the intestines of i-*Mcl1*$^{\Delta IEC}$ mice compared to those derived from i-*Apc*$^{\Delta IEC}$*Mcl1*$^{\Delta IEC}$ mice. Ex vivo culture of *Mcl1* deficient organoids was only possible with the added deletion of *Apc* indicating that the survival of *Mcl1* deficient ISC is dependent on the cell-intrinsic activation of WNT signaling. At the same time, we clearly show that in the presence of constitutive WNT signaling, *Mcl1* has a direct role in regulating ISC proliferation.

MCL1 deficient ISC, which retain OLFM4, *Lgr5* and SOX9 positivity, did not differentiate into the secondary secretory lineages as illustrated by a complete loss of both Paneth and goblet cells. This loss of differentiation is restricted to *Mcl1* deficient (phenotypic) regions of *Mcl1*$^{\Delta IEC}$ mice. Interestingly, *Mcl1* deficient ISC showed a significant reduction of the transcription factor *Atoh1*, essential for the differentiation to secondary secretory lineages[27]. However, ISC from *Mcl1*-expressing (non-phenotypic) areas retain high *Atoh1* expression levels and differentiate to Paneth and goblet cells at a similar rate to wild type ISC. The inability of MCL1 deficient ISC to differentiate to secretory cells was also observed under germ-free conditions, removing the potential influence of chronic inflammation. Whether or not this reduced *Atoh1* expression is a direct result of MCL1 deficiency or is a secondary effect of a WNT-signaling saturated environment deserves further investigation. These data suggest that MCL1 is essential for maintaining the strictly controlled balance between ISC proliferation and differentiation and the polarization of ISC towards a hyperproliferative state in the absence of MCL1 may facilitate genetic alterations predisposing to tumorigenesis.

Additionally, the strong positivity of γH2AX following *Mcl1* deletion within *Mcl1*$^{\Delta IEC}$ and i-*Mcl1*$^{\Delta IEC}$ mice may also be important in the context of tumor formation and further studies are

required to determine the significance of this observation. These γH2AX positive cells potentially represent IEC that had accumulated DNA damage but escaped apoptotic programming. DNA damage is a well-established hallmark of tumorigenesis[28], and following *Mcl1* deletion, may originate from the increased replicative stress. The potential role of MCL1 in maintaining DNA replication integrity is very intriguing and our findings support recent publications describing increased replicative stress and higher susceptibility to DNA double strand breaks[37, 38] and the strong synergistic effects of combining MCL1 and PARP-1 inhibitors to treat certain tumors[37, 39]. Collectively, these recent findings strongly suggest a non-redundant role for MCL1 in maintaining DNA replication integrity, the absence of which may result in DNA damage and potentially tumor initiation, as observed in *Mcl1*$^{\Delta IEC}$ mice.

Conceptually, these findings show that, depending on the context, MCL1 dysregulation can promote tumorigenesis by different means. On one hand, although very rare in human cancers[40], it is conceivable that early steps of carcinogenesis may be induced by severely impaired intestinal homeostasis resulting from, even transient, gene alterations and loss of MCL1 function. On the other hand, amplifications of chromosome 1 resulting in over-expression of MCL1[36, 41], a recurrent finding in a variety of cancers including CRC, is well known to confer a survival advantage within tumors[42]. Thus, pharmacologic inhibition of MCL1 recently has emerged as an attractive target to increase the susceptibility of different tumors to conventional anti-tumor therapies[39, 43, 44]. Although recently published MCL1 inhibitors have been shown to be tolerable and functional in a number of different cancer models[45, 46], intestinal pathology due to pharmacological inhibition of MCL1 has not yet been extensively addressed. A complete lack of adverse effects within the intestinal epithelium would be surprising given the MCL1 dependency of IEC shown in this study.

In summary, we not only demonstrate the crucial role for MCL1 in maintaining intestinal homeostasis, but also uncover an unexpected tumor suppressor capacity for MCL1 within the intestinal tract. These findings may contribute to unravelling the early stages of intestinal

cancer development, and may have important implications for current strategies aimed at pharmacologically targeting MCL1[45-47].

Acknowledgements

We would like to thank Marion Bawohl, Renaud Maire, Christiane Mittmann, Fabiola Prutek, Marcel Glönkler and André Fitsche for excellent technical assistance, as well as Massimo Lopes, Ruaidhri Jackson, Gerhard Rogler, Martin Hausmann and Andreas Diefenbach for sharing reagents and helpful discussion.

References

1. Peterson LW, Artis D. Intestinal epithelial cells: regulators of barrier function and immune homeostasis. Nat Rev Immunol 2014;14:141-53.
2. van der Flier LG, Clevers H. Stem cells, self-renewal, and differentiation in the intestinal epithelium. Annu Rev Physiol 2009;71:241-60.
3. Gunther C, Neumann H, Neurath MF, et al. Apoptosis, necrosis and necroptosis: cell death regulation in the intestinal epithelium. Gut 2013;62:1062-71.
4. Iwamoto M, Koji T, Makiyama K, et al. Apoptosis of crypt epithelial cells in ulcerative colitis. J Pathol 1996;180:152-9.
5. Karamchandani DM, Chetty R. Apoptotic colopathy: a pragmatic approach to diagnosis. J Clin Pathol 2018;71:1033-1040.
6. **Dannappel M, Vlantis K, Kumari S**, et al. RIPK1 maintains epithelial homeostasis by inhibiting apoptosis and necroptosis. Nature 2014;513:90-4.
7. **Lin J, Kumari S, Kim C**, et al. RIPK1 counteracts ZBP1-mediated necroptosis to inhibit inflammation. Nature 2016;540:124-128.
8. Gunther C, Martini E, Wittkopf N, et al. Caspase-8 regulates TNF-alpha-induced epithelial necroptosis and terminal ileitis. Nature 2011;477:335-9.
9. Newton K, Wickliffe KE, Maltzman A, et al. RIPK1 inhibits ZBP1-driven necroptosis during development. Nature 2016;540:129-133.
10. Takahashi N, Vereecke L, Bertrand MJ, et al. RIPK1 ensures intestinal homeostasis by protecting the epithelium against apoptosis. Nature 2014;513:95-9.
11. Welz PS, Wullaert A, Vlantis K, et al. FADD prevents RIP3-mediated epithelial cell necrosis and chronic intestinal inflammation. Nature 2011;477:330-4.
12. Scherr AL, Gdynia G, Salou M, et al. Bcl-xL is an oncogenic driver in colorectal cancer. Cell Death Dis 2016;7:e2342.
13. van der Heijden M, Zimberlin CD, Nicholson AM, et al. Bcl-2 is a critical mediator of intestinal transformation. Nat Commun 2016;7:10916.
14. Opferman JT, Iwasaki H, Ong CC, et al. Obligate role of anti-apoptotic MCL-1 in the survival of hematopoietic stem cells. Science 2005;307:1101-4.
15. **Weber A, Boger R**, Vick B, et al. Hepatocyte-specific deletion of the antiapoptotic protein myeloid cell leukemia-1 triggers proliferation and hepatocarcinogenesis in mice. Hepatology 2010;51:1226-36.
16. Boege Y, Malehmir M, Healy ME, et al. A Dual Role of Caspase-8 in Triggering and Sensing Proliferation-Associated DNA Damage, a Key Determinant of Liver Cancer Development. Cancer Cell 2017;32:342-359 e10.
17. Smith K, McCoy KD, Macpherson AJ. Use of axenic animals in studying the adaptation of mammals to their commensal intestinal microbiota. Semin Immunol 2007;19:59-69.
18. **Grivennikov SI, Wang K**, Mucida D, et al. Adenoma-linked barrier defects and microbial products drive IL-23/IL-17-mediated tumour growth. Nature 2012;491:254-8.
19. Fredenburgh LE, Velandia MM, Ma J, et al. Cyclooxygenase-2 deficiency leads to intestinal barrier dysfunction and increased mortality during polymicrobial sepsis. J Immunol 2011;187:5255-67.
20. Boivin GP, Washington K, Yang K, et al. Pathology of mouse models of intestinal cancer: consensus report and recommendations. Gastroenterology 2003;124:762-77.
21. Fred T. Bosman FC, Ralph H. Hruban, Neil D. Theise. Tumours of the colon and rectum. WHO Classification of Tumours of the Digestive System. Volume 4th Edition: WHO Press, 2010:140-142.
22. Zenewicz LA, Yancopoulos GD, Valenzuela DM, et al. Innate and adaptive interleukin-22 protects mice from inflammatory bowel disease. Immunity 2008;29:947-57.
23. Sansom OJ, Reed KR, Hayes AJ, et al. Loss of Apc in vivo immediately perturbs Wnt signaling, differentiation, and migration. Genes Dev 2004;18:1385-90.

24. Van der Flier LG, Sabates-Bellver J, Oving I, et al. The Intestinal Wnt/TCF Signature. Gastroenterology 2007;132:628-32.
25. Moor AE, Harnik Y, Ben-Moshe S, et al. Spatial Reconstruction of Single Enterocytes Uncovers Broad Zonation along the Intestinal Villus Axis. Cell 2018;175:1156-1167.e15.
26. Artis D, Spits H. The biology of innate lymphoid cells. Nature 2015;517:293-301.
27. Yang Q, Bermingham NA, Finegold MJ, et al. Requirement of Math1 for secretory cell lineage commitment in the mouse intestine. Science 2001;294:2155-8.
28. Zeman MK, Cimprich KA. Causes and consequences of replication stress. Nat Cell Biol 2014;16:2-9.
29. Jackstadt R, Sansom OJ. Mouse models of intestinal cancer. J Pathol 2016;238:141-51.
30. Fearon ER, Vogelstein B. A genetic model for colorectal tumorigenesis. Cell 1990;61:759-67.
31. **Schepers AG, Snippert HJ**, Stange DE, et al. Lineage tracing reveals Lgr5+ stem cell activity in mouse intestinal adenomas. Science 2012;337:730-5.
32. Cancer Genome Atlas N. Comprehensive molecular characterization of human colon and rectal cancer. Nature 2012;487:330-7.
33. **Liu Y, Sethi NS, Hinoue T**, et al. Comparative Molecular Analysis of Gastrointestinal Adenocarcinomas. Cancer Cell 2018;33:721-735.e8.
34. Grivennikov SI, Greten FR, Karin M. Immunity, inflammation, and cancer. Cell 2010;140:883-99.
35. **Choi CR, Bakir IA**, Hart AL, et al. Clonal evolution of colorectal cancer in IBD. Nat Rev Gastroenterol Hepatol 2017;14:218-229.
36. Perciavalle RM, Opferman JT. Delving deeper: MCL-1's contributions to normal and cancer biology. Trends Cell Biol 2013;23:22-9.
37. Chen G, Magis AT, Xu K, et al. Targeting Mcl-1 enhances DNA replication stress sensitivity to cancer therapy. J Clin Invest 2018;128:500-516.
38. Mattoo AR, Pandita RK, Chakraborty S, et al. MCL-1 Depletion Impairs DNA Double-Strand Break Repair and Reinitiation of Stalled DNA Replication Forks. Mol Cell Biol 2017;37.
39. Annunziato S, de Ruiter JR, Henneman L, et al. Comparative oncogenomics identifies combinations of driver genes and drug targets in BRCA1-mutated breast cancer. Nat Commun 2019;10:397.
40. **Beroukhim R, Mermel CH**, Porter D, et al. The landscape of somatic copy-number alteration across human cancers. Nature 2010;463:899-905.
41. Juin P, Geneste O, Gautier F, et al. Decoding and unlocking the BCL-2 dependency of cancer cells. Nat Rev Cancer 2013;13:455-65.
42. Hanahan D, Weinberg RA. Hallmarks of cancer: the next generation. Cell 2011;144:646-74.
43. Pan R, Ruvolo VR, Wei J, et al. Inhibition of Mcl-1 with the pan-Bcl-2 family inhibitor (-)BI97D6 overcomes ABT-737 resistance in acute myeloid leukemia. Blood 2015;126:363-72.
44. Hird AW, Tron AE. Recent advances in the development of Mcl-1 inhibitors for cancer therapy. Pharmacol Ther 2019.
45. Kotschy A, Szlavik Z, Murray J, et al. The MCL1 inhibitor S63845 is tolerable and effective in diverse cancer models. Nature 2016;538:477-482.
46. Tron AE, Belmonte MA, Adam A, et al. Discovery of Mcl-1-specific inhibitor AZD5991 and preclinical activity in multiple myeloma and acute myeloid leukemia. Nat Commun 2018;9:5341.
47. Xiang W, Yang CY, Bai L. MCL-1 inhibition in cancer treatment. Onco Targets Ther 2018;11:7301-7314.

Author names in bold designate shared co-first authorship

Figure 1: MCL1 is essential for maintaining intestinal homeostasis. (*A*) *Mcl1*$^{\Delta IEC}$ mice show reduced weight gain (n=50) and survival (n=126) compared to littermate controls (n=34 and n=61 respectively). Representative colonoscopy images from 4-month-old mice. (*B*) 2-month-old *Mcl1*$^{\Delta IEC}$ mice display increased FITC-dextran (n=13) compared with littermate controls (n=8) 4 hours after oral administration. (*C*) Calprotectin (S100A8/S100A9) levels of 2-month-old *Mcl1*$^{\Delta IEC}$ mice and age-matched controls by ELISA (n=6 *Mcl1*$^{\Delta IEC}$ mice, n=9 wild type) or real time PCR (n=8 *Mcl1*$^{\Delta IEC}$ mice, n=5 wild type). (*D*) Representative images illustrating *Mcl1* expression in the colon (red stain) as demonstrated using ISH (scale bars: 100μm). (*E*) Representative images from the colon of 2-month-old *Mcl1*$^{\Delta IEC}$ mice compared with age-matched controls (scale bars: 100μm , 25μm-inserts). (*F*) Blinded histological scores comparing the colon of 2-month-old *Mcl1*$^{\Delta IEC}$ mice with littermate controls (n=5). (*G*) Colon cultures established from 2-month-old mice and analysed using multiplex analysis (minimum n=10 per group). Data presented as either bar charts or scatter plot graph show mean values ± s.e.m. Statistical analyses were conducted by one-way ANOVA with Bonferroni correction (*A* (body weight), *G*), log rank (Mantel-Cox test) (*A*, survival), student's t-test (*B* and *C*), or Mann-Whitney test (*F*) where * $p \leq 0.05$, ** $p \leq 0.01$, *** $p \leq 0.001$.

Figure 2: MCL1 deficiency-associated chronic inflammation is mediated by ILC. (*A*) Genetic depletion of *Rag1* within *Mcl1*$^{\Delta IEC}$ mice significantly reduced weight gain and survival (n=19). Blue asterisk: *Mcl1*$^{\Delta IEC}$ mice compared to littermate controls, red asterisk: *Mcl1*$^{\Delta IEC}$*Rag1*$^{-/-}$ mice compared to littermate controls, purple asterisk: *Mcl*1$^{\Delta IEC}$ mice compared with *Mcl1*$^{\Delta IEC}$*Rag1*$^{-/-}$ mice. (*B*) Representative images from the colon of 2-month-old *Rag*1$^{-/-}$ control mice compared with *Mcl1*$^{\Delta IEC}$*Rag*1$^{-/-}$ mice showing impaired intestinal architecture (H&E), increased IEC apoptosis (cl. casp. 3) and hyperproliferation (Ki-67) (scale bars: 100μm, 25μm-inserts). (*C*) Blinded histological scores comparing 2-month-old *Mcl1*$^{\Delta IEC}$*Rag1*$^{-/-}$ mice with *Rag*1$^{-/-}$ mice (n=5). (*D*) Colon cultures established from 2-month-old mice and analysed using multiplex analysis (minimum n=8 per group). (*E*) Representative images from colons of 3-month-old *Mcl1*$^{\Delta IEC}$*Rag1*$^{-/-}$ mice following 4 weeks of α-Thy1.2 depleting antibody or corresponding isotype administration (scale bars: 100μm, 25μm-inserts). (*F*) Colon cultures established from 3-month-old mice and analysed for TNF-α, IL-22, IL-23A, IL-17A, IL-17F and IL-1β expression using multiplex analysis (minimum n=8 per group). Data presented as either bar charts or scatter plot graph show mean values ± s.e.m. Statistical analyses were conducted by one-way ANOVA with Bonferroni correction (*A* (body weight), *D* and *F*), log rank (Mantel-Cox test) (*A*, survival) or Mann-Whitney test (*C*) where * $p \leq 0.05$, ** $p \leq 0.01$, *** $p \leq 0.001$.

Figure 3: IEC apoptosis and hyperproliferation are a direct consequence of *Mcl1* deletion. (*A*) Representative images from the colon of 2-month-old germ-free *Mcl1*$^{\Delta IEC}$ mice compared with littermate controls illustrating increased IEC apoptosis (cl. casp. 3) and hyperproliferation (Ki-67) (scale bars: 100μm, 25μm-inserts). (*B*) Blinded histological scores comparing 2-month-old *Mcl1*$^{\Delta IEC}$ mice with littermate controls under germ-free conditions (n=5 per group). (*C*) Colon cultures established from 2-month-old germ-free mice and analysed using multiplex analysis (minimum n=15 per group). Data presented as either bar charts or scatter plot graphs represents mean values ± s.e.m. Statistical analyses were conducted by Mann-Whitney test (*B*) or by one-way ANOVA with Bonferroni correction (*C*) where * $p \leq 0.05$.

Figure 4: MCL1 is essential for ISC differentiation. (*A*) Representative images from the small intestine of 2-month-old *Mcl1*$^{\Delta IEC}$ mice compared with age matched controls illustrating impaired goblet (AB/PAS) and Paneth cell (Lysozyme) differentiation, increased proliferation (Ki-67) and retention of stem cell markers (OLFM4 and SOX9) (scale bars: 100μm). (*B*) Quantification of total goblet (AB/PAS) and Paneth cells (Lysozyme) in the small intestine. (*C*) Quantification of total goblet (AB/PAS) cells in the colon. (*D*) Representative images from the small intestine of *Mcl1*$^{\Delta IEC}$ mice visualising *Atoh1* expression in *Mcl1*-positive versus *Mcl1*-deficient IEC using smFISH. White dots represents single molecules of *Atoh1* while red dots represent *Mcl1*. * indicates overexposed non-specific signal. Green boxes mark the areas shown in higher magnification below (scale bars: 25μm-upper, 10μm-lower). (*E*) Quantificaiton of *Atoh1* smFISH signal (n=7 per group). Data presented as either bar charts or scatter plot graph show mean values ± s.e.m. Statistical analyses were conducted by Mann-Whitney test (*B, C* and *E*) where *** $p \leq 0.001$

Figure 5: MCL1 protects the small intesitne from activating WNT signalling and DNA damage. (*A*-*B*) Representative images from the small intestine of i-*Mcl1*$^{\Delta IEC}$ mice and age-matched controls, (4 days post induction) (scale bars: 100μm, 25μm-insert). (*C*) Gene Set Enrichment Analysis (GSEA) carried out on RNA sequencing data from i-*Mcl1*$^{\Delta IEC}$ mouse compared with littermate controls. (*D*) GSEA analysis tested for WNT target genes commonly up-regulated in human CRC (upper) or in i-*Apc*$^{\Delta IEC}$ mouse models (lower). (*E*) BrdU staining from the small intestines of wild type, i-*Ctnnb1*$^{\Delta IEC/wt}$, i-*Mcl1*$^{\Delta IEC}$ and i-*Ctnnb1*$^{\Delta IEC/wt}$*Mcl1*$^{\Delta IEC}$ mice,4 days post induction (scale bars: 100μm). Quantification of BrdU staining (positive cells/half crypt) is shown below (n=3). (*F*) BrdU staining from the small intestines of vehicle treated wild type and i-*Mcl1*$^{\Delta IEC}$ mice compared with their WNT974 treated counterparts, 3 days post induction (scale bars: 100μm). Quantification of BrdU staining (positive cells/half crypt) is shown below (n=3). (*G*) Representative images from the small intestine of *Mcl1*$^{\Delta IEC}$ mice visualising *Wnt2b* expression in *Mcl1*-positive versus *Mcl1*-deficient IEC using smFISH. White dots represents single molecules of *Wnt2b* while red dots represent *Mcl1.* * indicates overexposed non-specific signal. Green dashed lines represents the perimeter of intestinal crypts (scale bars: 25μm-lower magnification, 10μm-higher magnification). All data presented as scatter plot graph represents mean values ± s.e.m. Statistical analysis was conducted by Mann-Whitney test (*E* and *F*) where * $p \leq 0.05$.

Figure 6: MCL1 is an essential regulator of IEC proliferation. (*A*) Representative images of small intestinal or colonic tissue from i-*Apc*$^{\Delta IEC}$ and i-*Apc*$^{\Delta IEC}$*Mcl1*$^{\Delta IEC}$ mice (3 days post induction), and stained with H&E or for BrdU (scale bar: 50μm). Quantification of BrdU positive cells per half crypt from small intestine and colon (right panel). Normalised expression of *Pcna* (*B*), *Cdk1* (*C*) and *Cdk4* (*D*) in whole small intestine tissue from wild type controls and i-*Mcl1*$^{\Delta IEC}$ mice (4 post induction), or i-*Apc*$^{\Delta IEC}$ and i-*Apc*$^{\Delta IEC}$*Mcl1*$^{\Delta IEC}$ mice (3 post induction) and analysed by RNAseq (n=3 per group). (*E*) Normalised expression of *Mcl1* in whole small intestinal tissue at day 4 post induction (left) or small intestine derived organoids at passage ≥3 (right) from wild type or i-*Mcl1*$^{\Delta IEC}$ mice as analysed by RNAseq (n=3 per group). (*F*) Relative expression of *Mcl1* in whole small intestinal tissue at day 3 post induction (left) or small intestine derived organoids at passage ≥5 (right) in i-*Apc*$^{\Delta IEC}$ or i-*Apc*$^{\Delta IEC}$*Mcl1*$^{\Delta IEC}$ mice as analysed by RNAseq (n=3 per group). (*G*) Representative images of small intestine derived organoids from i-*Apc*$^{\Delta IEC}$ or i-*Apc*$^{\Delta IEC}$*Mcl1*$^{\Delta IEC}$ mice (100x). All data presented as scatter plot graph represents mean values ± s.e.m. Statistical analysis was conducted by one-tailed Mann-Whitney test where * $p \leq 0.05$.

Figure 7: MCL1 protects from intestinal carcinoma development. (*A*) Representative images from colonoscopies (top), macroscopic imaging (bottom) and H&E characterisation of colon carcinoma found in 18-month-old *Mcl1*$^{\Delta IEC}$ mouse (scale bar: 500μm) (right). (*B*) Percentage and classification of tumor lesions observed in 12-month-old SPF *Mcl1*$^{\Delta IEC}$ mice (n=42) compared with germ-free *Mcl1*$^{\Delta IEC}$ mice (n=12). White sections: no tumor lesions or mucosal hyperplasia, light grey sections: low-grade adenomas (LGA), dark grey sections: high-grade adenomas (HGA), black sections: carcinoma (CA). In cases where more than a single lesion was present, individual mice were classified according to the highest tumor lesion. (*C*) IHC staining illustrating the invasive growth of carcinoma in *Mcl1*$^{\Delta IEC}$ mice. Carcinoma cells, α-SMA negative (black boxes) and cytokeratin positive (black arrow heads), actively invade the *muscularis propria* of a 18-month-old *Mcl1*$^{\Delta IEC}$ mouse (scale bar: 100μm scale bars). Black circle indicates vesicular invasion. (*D*) IHC analysis showing lack of MCL1 expression in tumors that develop in *Mcl1*$^{\Delta IEC}$ mice (scale bar: 100μm-upper, 25μm-lower). (*E*) ISH for WNT target gene *Axin2* (scale bar: 100μm-upper, 50μm-lower). (*F*) Representative IHC staining illustrating nuclear β-catenin localisation (white arrow heads) observed in a carcinoma from a 12-month-old *Mcl1*$^{\Delta IEC}$ mouse (scale bar: 100μm-upper, 25μm-lower). Below, a heterozygous missense point mutation in a mutational hot spot region of exon 2 of *Ctnnb1* (NM_000075.6:c.98C>T - p.Ser33Phe) (3/5 carcinomas sequenced). (*G*) aCGH analysis of tumors isolated from 12-month-old *Mcl1*$^{\Delta IEC}$ mice (from left to right: 8 carcinoma samples, 2 adenoma samples and 2 unaffected samples from 18-month-old *Mcl1*$^{\Delta IEC}$ mice). (*H*) Synteny analysis comparing chromosomal aberrations in carcinomas from *Mcl1*$^{\Delta IEC}$ mice with human CRC (Murine chromosomes: M1-M19; Human chromosomes H1-H22). Statistical analyses for non-random distribution of matched copy number gains revealed $p<0.0001$ for both gains and losses.

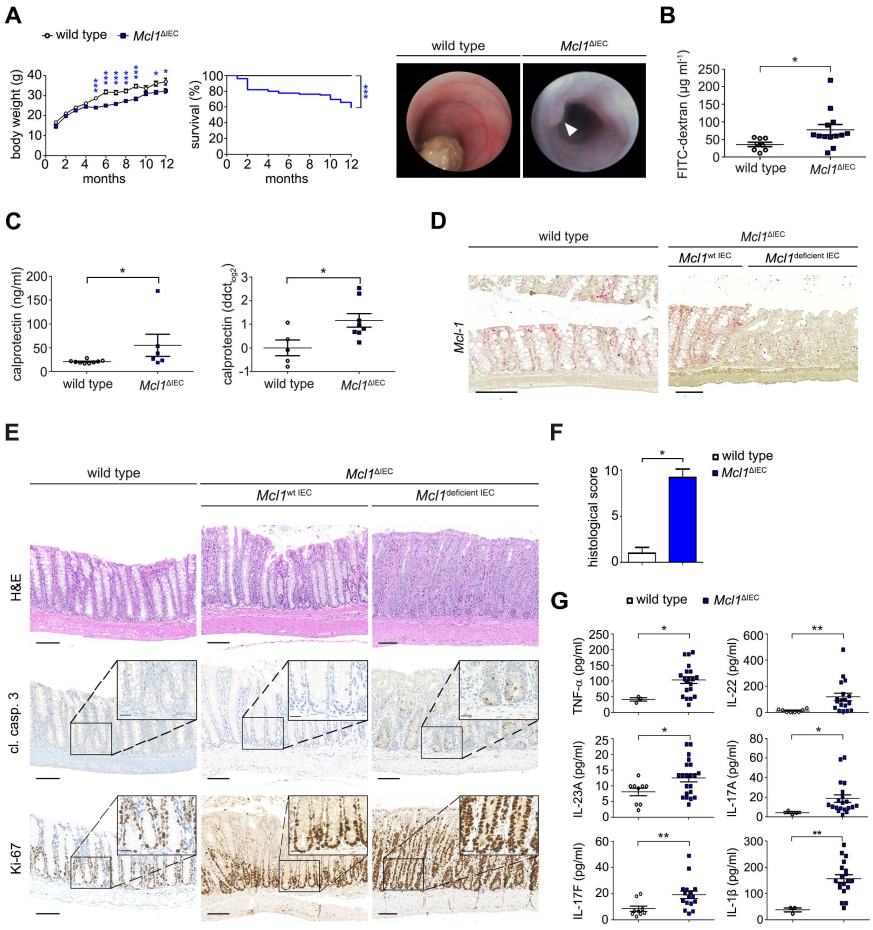

Figure 1. Healy*, Boege*, Hodder* et al.

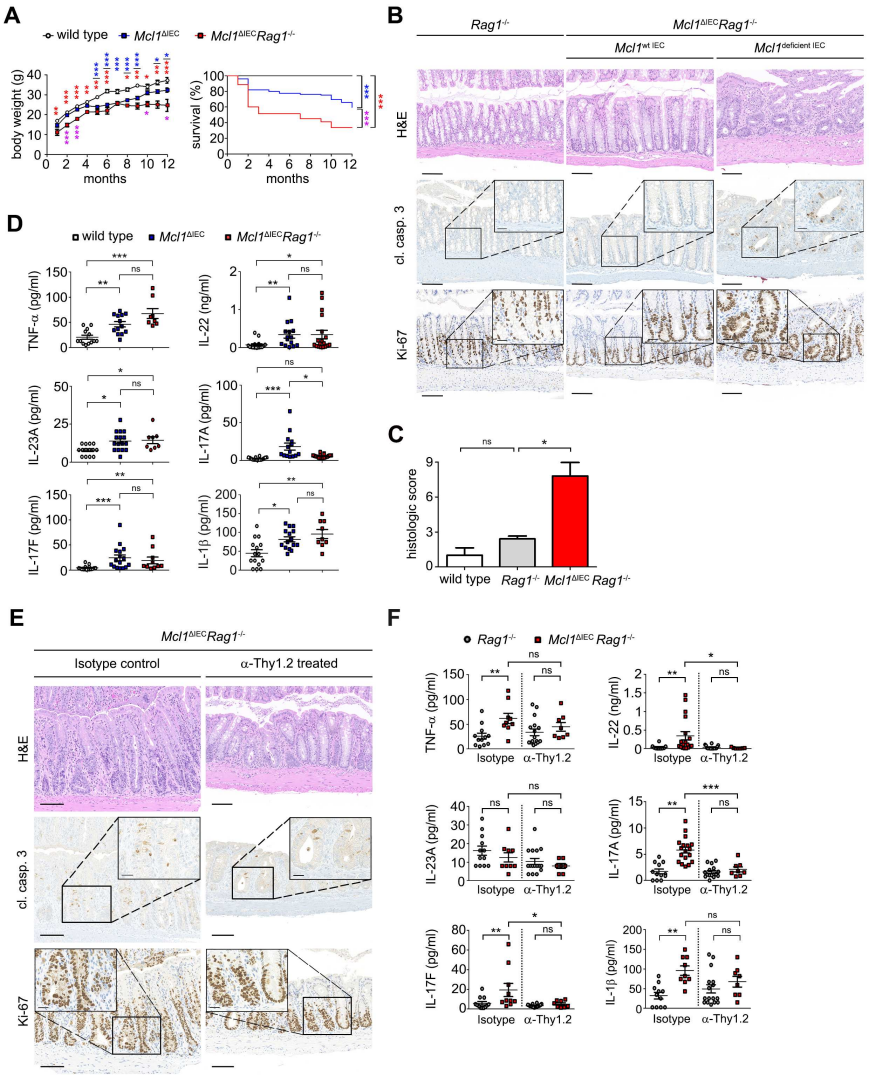

Figure 2. Healy*, Boege*, Hodder* et al.

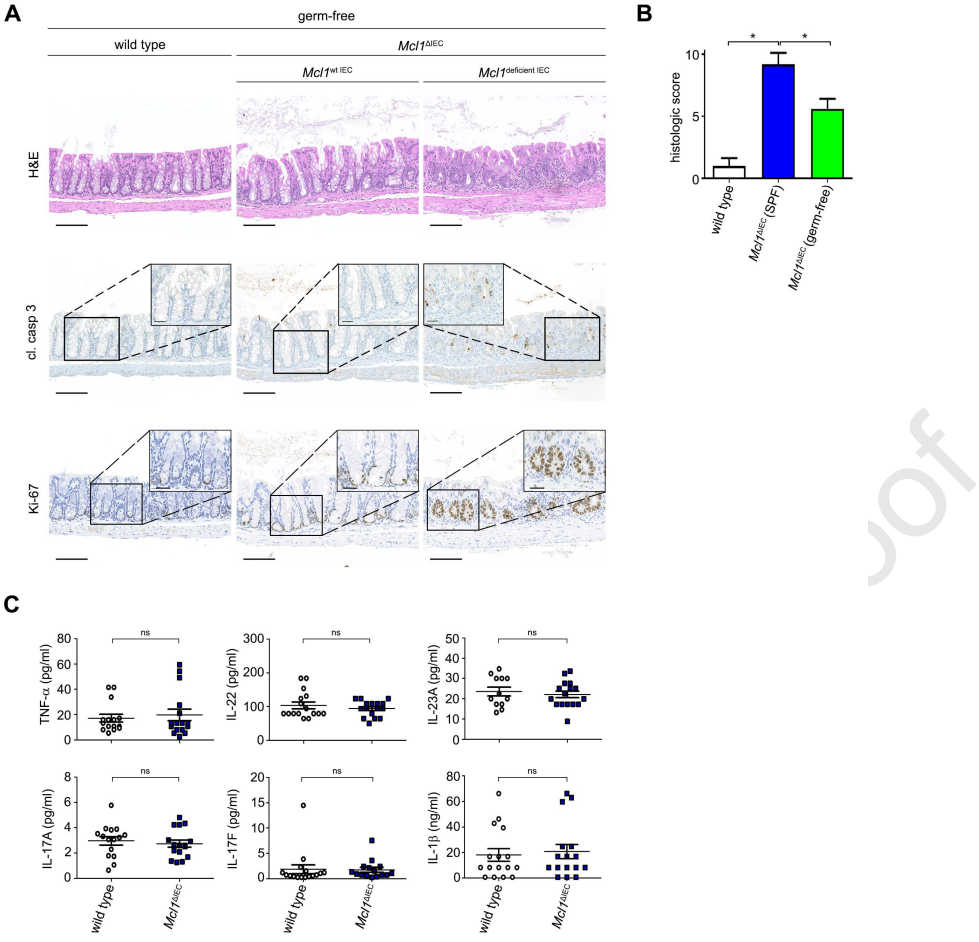

Figure 3. Healy*, Boege*, Hodder* et al.

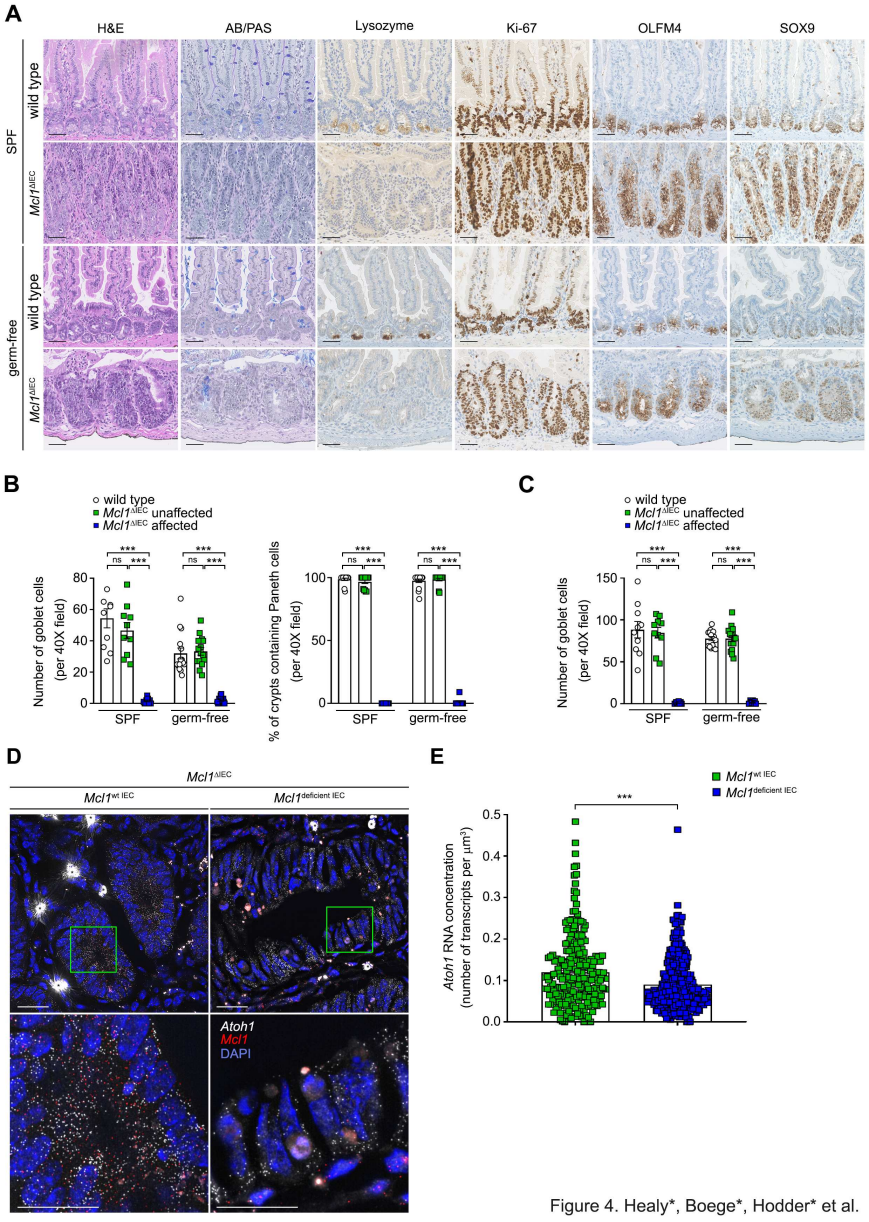

Figure 4. Healy*, Boege*, Hodder* et al.

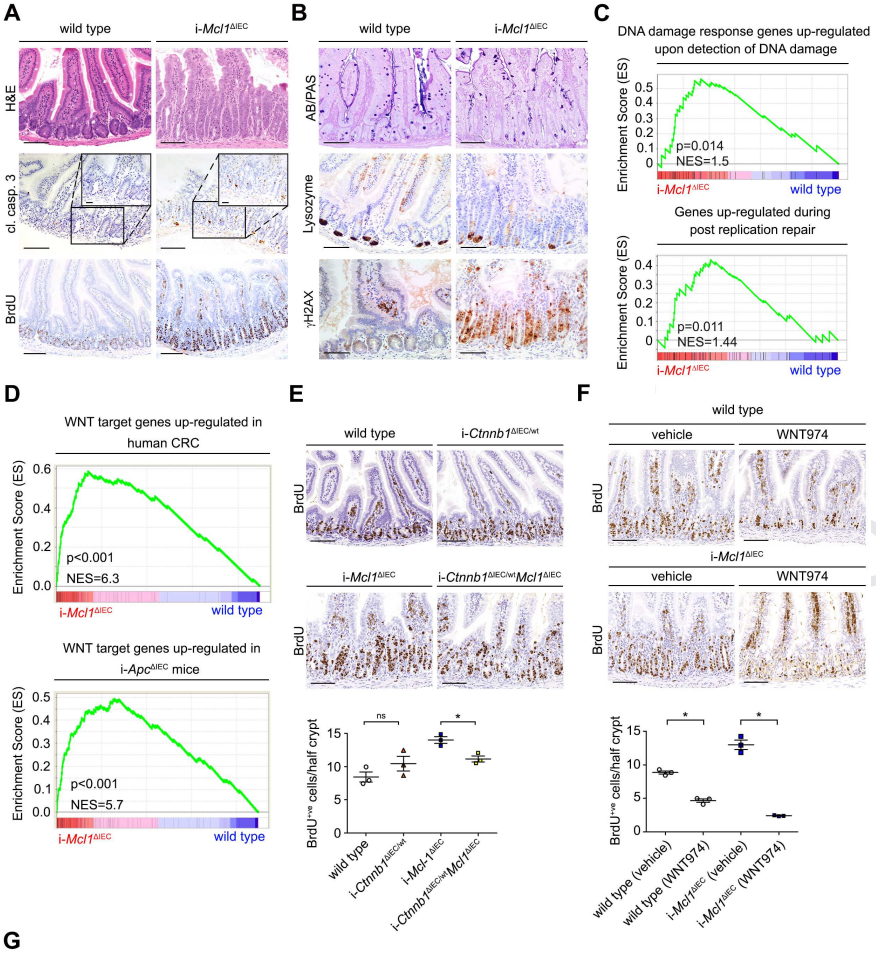

Figure 5. Healy*, Boege*, Hodder* et al.

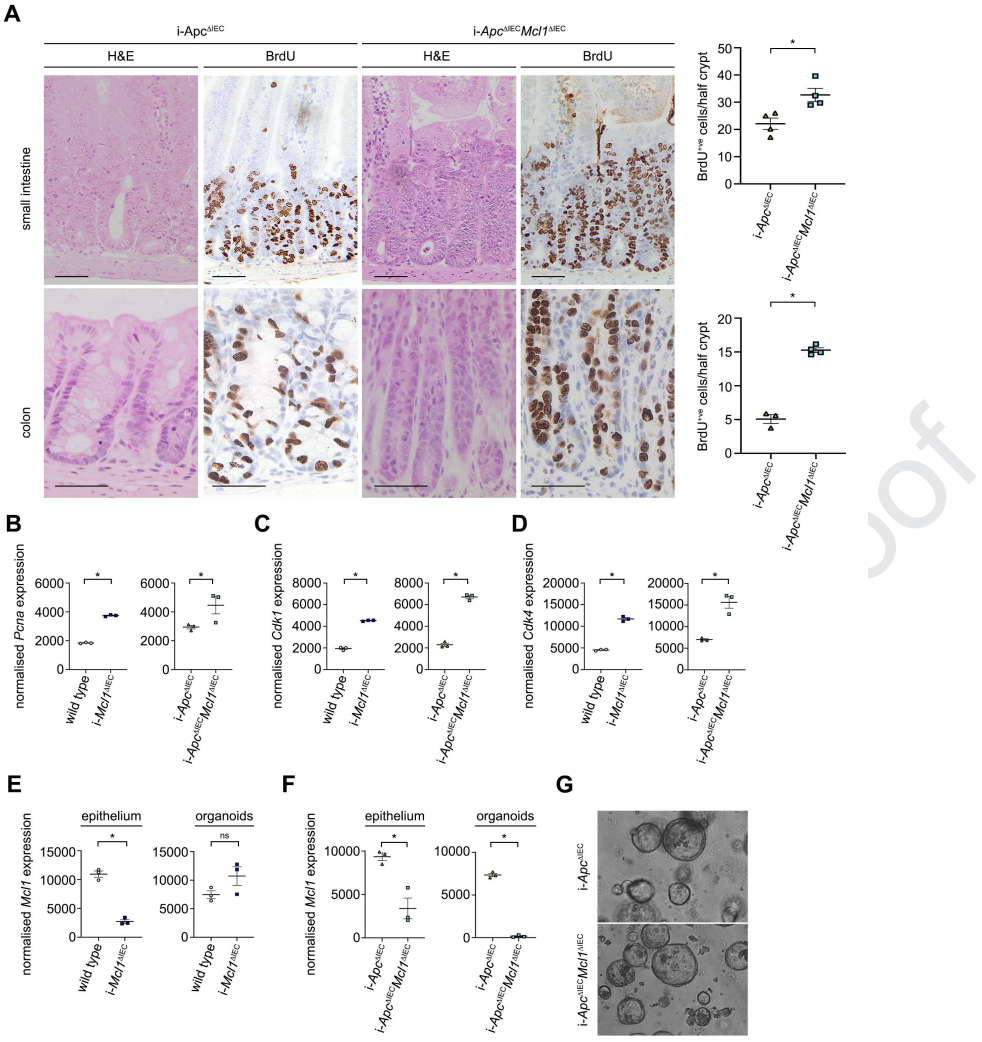

Figure 6. Healy, Boege, Hodder *et. al*

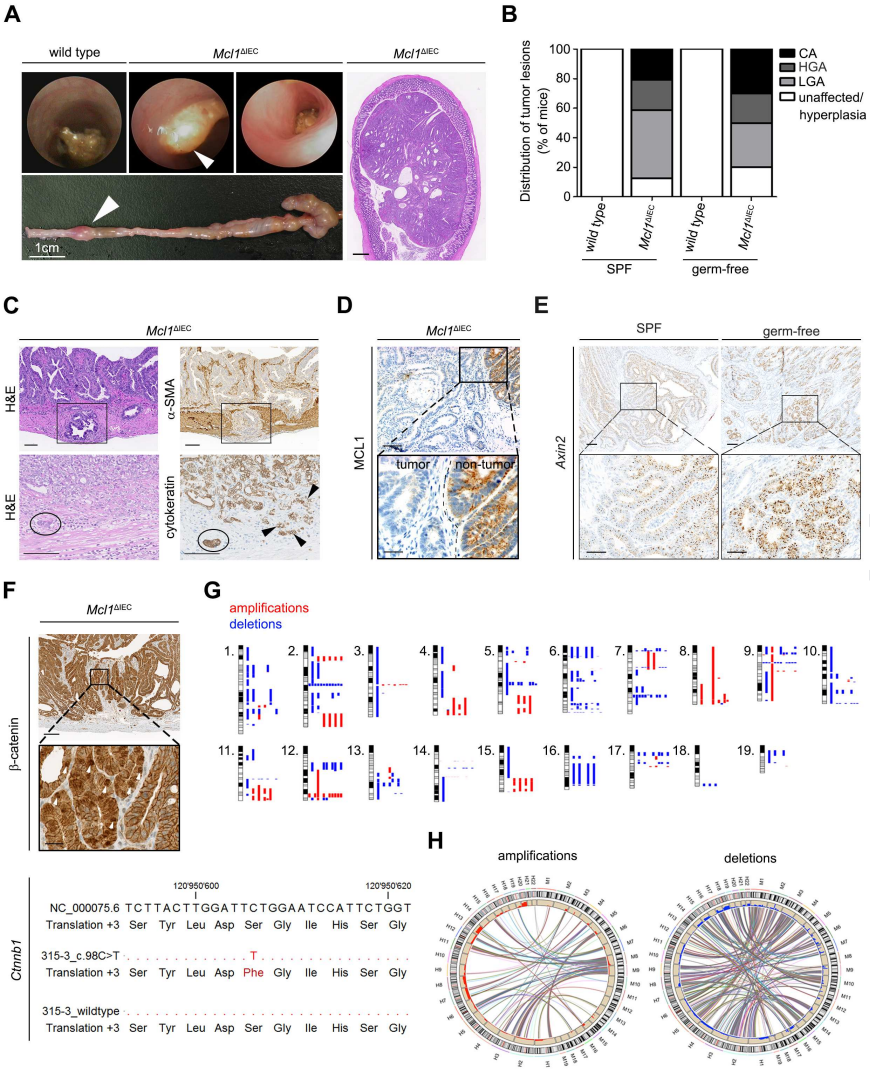

Figure 7. Healy*, Boege*, Hodder* et al.

What you need to know:

BACKGROUND AND CONTEXT: Intestinal epithelial homeostasis depends on a tightly regulated balance between intestinal epithelial cell (IEC) death and proliferation. Disruption of factors that regulate IEC death result in intestinal inflammation, whereas loss of anti-apoptotic proteins, such as family members BCL2 and BCL2L1, have no effects on intestinal homeostasis in mice,

NEW FINDINGS: The BCL2 family member MCL1 is required for maintenance of intestinal homeostasis and prevention of carcinogenesis in mice. Loss of MCL1 results in intestinal carcinogenesis—even under germ-free conditions, and therefore does not involve microbe-induced chronic inflammation.

LIMITATIONS: This study was performed in mice. Studies are needed to determine whether MCL1 function is disrupted in patients with inflammatory bowel diseases or cancer.

IMPACT: *Mcl1*$^{\Delta IEC}$ mice might be used to study apoptotic enterocolopathy and inflammatory bowel diseases.

Lay Summary:

We identified a protein, MCL1, that regulates proliferation of intestinal epithelial cells. Its loss might promote development of intestinal cancer.